5676 J. Med. Chem. 2010, 53, 5676–5683
DOI: 10.1021/jm100421n

Journal of Medicinal Chemistry Article

Structural Basis for Inhibition of Eg5 by Dihydropyrimidines: Stereoselectivity of Antimitotic Inhibitors Enastron, Dimethylenastron and Fluorastrol†

Hung Yi Kristal Kaan,‡ Venkatasubramanian Ulaganathan,‡ Oliver Rath,‡ Hana Prokopcová,§ Doris Dallinger,§ C. Oliver Kappe,§ and Frank Kozielski*,‡

‡The Beatson Institute for Cancer Research, Garscube Estate, Switchback Road, Bearsden, Glasgow G61 1BW, Scotland, U.K., and §Institute of Chemistry, Karl-Franzens-University Graz, Heinrichstrasse 28, 8010 Graz, Austria

Received April 6, 2010

Human kinesin Eg5, which plays an essential role in mitosis by establishing the bipolar spindle, has proven to be an interesting drug target for the development of cancer chemotherapeutics. Here, we report the crystal structures of the Eg5 motor domain complexed with enastron, dimethylenastron, and fluorastrol. By comparing these structures to that of monastrol and mon-97, we identified the main reasons for increased potency of these new inhibitors, namely the better fit of the ligand to the allosteric binding site and the addition of fluorine atoms. We also noticed preferential binding of the *S*-enantiomer of enastron and dimethylenastron to Eg5, while the *R*-enantiomer of fluorastrol binds preferentially to Eg5. In addition, we performed a multidrug resistance (MDR) study in cell lines overexpressing P-glycoprotein (Pgp). We showed that one of these inhibitors may have the potential to overcome susceptibility to this efflux pump and hence overcome common resistance associated with tubulin-targeting drugs.

Introduction

Human Eg5 is a member of the kinesin superfamily and is responsible for the formation of mitotic spindles.[1] Current models suggest that Eg5 separates the duplicated centrosomes by pushing antiparallel microtubules apart, thus establishing the bipolar spindle.[2,3] Eg5 is an interesting candidate for drug development in cancer chemotherapy because its inhibition causes cells to arrest in mitosis with the characteristic phenotype of monoastral spindles.[1,4,5] Activation of the mitotic checkpoint then leads to prolonged mitotic arrest and subsequent apoptotic cell death in certain tumor cell lines.

While conducting an elegant phenotype-based screen for small molecules that inhibit the formation of the bipolar spindle, Mayer et al. discovered a compound called monastrol, which specifically inhibits the motility of Eg5.[5] Prior to monastrol, all small molecules that affected the mitotic machinery targeted tubulin, the building block of microtubules. Taxanes and vinca alkaloids, which target tubulin and microtubules and interfere with microtubule dynamics, are widely used as efficient anticancer drugs for more than a decade.[6] Although these drugs possess antitumor properties by impeding mitosis and cell proliferation, patients treated with these drugs also suffer from microtubule-dependent side effects such as peripheral neuropathy.[7]

Given the risk of neurotoxicity caused by these drugs and the development of drug resistance by tumor cells, alternatives to microtubule-based drugs are greatly desired. Currently, Eg5 has received much attention as a target for drug development in cancer therapy, with seven inhibitors already in phase I or II clinical trials and several more in development.[8] Much of the effort has been geared toward designing inhibitors that are more potent and more specific to reduce dose-dependent toxicity and undesired side effects.

So far, two structures of Eg5 in complex with dihydropyrimidine (DHPM[a])-derived inhibitors have been solved[9,10] and employed for structure-based drug development. An initial SAR study by Gartner et al.[11] led to the discovery of new DHPM analogues such as enastron and dimethylenastron (Figure 1); the latter displaying improved potency in vitro and in cell-based assays. A point to note is the addition of the dimethyl group to enastron results in a 10-fold increase in potency. However, a further study by the same group did not yield any improvement to the first series of inhibitors.[12] Although these inhibitors have drug-like properties, relatively little has been published in the literature about the development of more potent DHPM analogues. DHPM inhibitors are unusual in the sense that both the *S*-enantiomer in the case for monastrol[9] and the *R*-enantiomer in the case of mon-97[10] have been identified as the biological active agents with two different binding modes. Studies on DHPM analogues have not clarified whether the *S*- or the *R*-enantiomer is the active agent; thus, making further improvement of these compounds difficult.

Further improvement of DHPMs would require broad structural information and the knowledge of the configuration

†PDB ID: 2X7C (Eg5-*S*-enastron), 2X7D (Eg5-*S*-dimethylenastron), and 2X7E (Eg5-*R*-fluorastrol).

*To whom correspondence should be addressed. Phone: +44-141-330-3186. Fax: +44-141-942-6521. E-mail: f.kozielski@beatson.gla.ac.uk.

[a] Abbreviations: IC_{50}, half maximal inhibitory concentration; DHPM, dihydropyrimidine; SAR, structure−activity relationship; DMEM, Dulbecco's Modified Eagle Medium; EC_{50}, half maximal effective concentration; MDR, multidrug resistance; PDB, Protein Data Bank; Pgp, P-glycoprotein; DMSO, dimethyl sulfoxide.

 Published on Web 07/02/2010

of DHPMs bound in the inhibitor-binding pocket of Eg5. To this end, we have solved the crystal structures of two DHPM analogues, enastron and dimethylenastron, in complex with Eg5. We have also solved the crystal structure of Eg5 in complex with a new 5-aroyl-DHPM derivative, fluorastrol (Figure 1), which is the most active DHPM compound identified from our SAR study.[13] We then tested the potency of a series of inhibitor analogues in a variety of cell lines. Two of the most potent analogues were also investigated to determine whether they are substrates for the P-glycoprotein (Pgp) efflux pumps by determining their multidrug resistance (MDR) ratios in two different epithelial cell lines overexpressing human Pgp.

Materials and Methods

Protein Expression and Purification. The motor domain of human Eg5 (residues 1−368) was cloned, expressed, and purified as previously described.[14]

Synthesis of Inhibitor Analogues. Enastron and dimethylenastron were synthesized according to published protocols.[11] Synthesis of mon-97 and its separation into enantiomers were performed as previously described.[10] Fluorastrol (Fluor = fluorine; astrol = aster, star) and related analogues (**1** and **2**) were prepared by standard Biginelli multicomponent reaction in analogy to published procedures for similar analogues.[10,11,13]

Crystallization of Eg5−Inhibitor Complexes. Purified Eg5 was incubated with 2 mM of each inhibitor in DMSO separately for 1 h on ice and centrifuged at 13000 rpm for 5 min at 4 °C to pellet undissolved inhibitor before setting up of crystal trays. Crystals

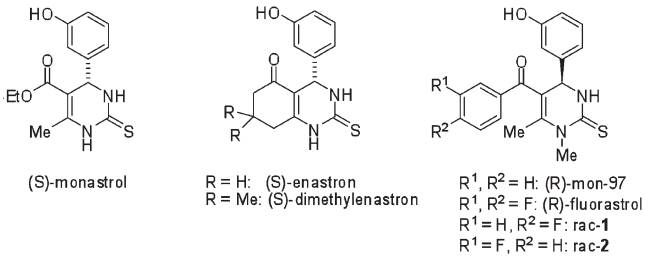

Figure 1. Chemical structures of DHPMs as inhibitors of mitotic kinesin Eg5: *S*-monastrol, *S*-enastron, *S*-dimethylenastron, *R*-mon-97, *R*-fluorastrol, *rac*-**1**, and *rac*-**2**.

of Eg5 with enastron appeared 2 days after microseeding crystals of Eg5 with monastrol into hanging-drops of 1 μL of Eg5−enastron complex (10 mg/mL) mixed with 1 μL of reservoir solution containing 25% polyethylene glycol-3350, 0.2 M K_2HPO_4, and 0.1 M HEPES pH 8.0 in VDX plates (Hampton Research) at 4 °C. A hexagonal-shaped crystal with dimensions of approximately 0.1 mm × 0.1 mm × 0.1 mm was immersed in cryoprotectant solution (30% polyethylene glycol-3350, 0.24 M K_2HPO_4, 0.12 M HEPES pH 8.0, 60 mM KCl, and 20% erythritol) and flash frozen in liquid nitrogen.

Crystals of Eg5 with dimethylenastron crystallized four days after microseeding crystals of Eg5 with monastrol into hanging-drops of 1 μL of Eg5−dimethylenastron complex (10 mg/mL) mixed with 1 μL of reservoir solution containing 28% polyethylene glycol-3350, 0.2 M K_2HPO_4, and 0.1 M HEPES pH 6.5 in VDX plates at 4 °C. Hexagonal-shaped crystals with dimensions of approximately 0.1 mm × 0.1 mm × 0.1 mm were immersed in cryoprotectant solution (33.6% polyethylene glycol-3350, 0.24 M K_2HPO_4, 0.12 M HEPES pH 6.5, 60 mM KCl, and 20% erythritol) and flash frozen in liquid nitrogen.

Crystals of Eg5 with racemic fluorastrol appeared after 1 day in hanging drops by mixing 1 μL of protein−inhibitor complex (10 mg/mL) with 1 μL of reservoir solution containing 30% polyethylene glycol-3350, 0.2 M K_2HPO_4, and 0.1 M HEPES pH 8.0 in VDX plates (Hampton Research) at 4 °C. A block-shaped crystal with dimensions of approximately 0.1 mm × 0.1 mm × 0.1 mm was immersed in cryoprotectant solution (30% polyethylene glycol-3350, 0.24 M K_2HPO_4, 0.12 M HEPES pH 8.0, 0.3 M NaCl, and 20% erythritol) and flash frozen in liquid nitrogen.

Data Collection and Processing. The diffraction data of the Eg5−enastron and Eg5−dimethylenastron crystals were measured at the European Synchrotron Radiation Facility, ESRF, on ID23−1. The diffraction data for the Eg5−fluorastrol crystal was measured at beamline ID14−1. The data for Eg5−fluorastrol was processed using HKL2000/Scalepack;[15] the data for Eg5−enastron and Eg5−dimethylenastron were processed using MOSFLM[16] and scaled using Scala from the CCP4 suite of programs.[17]

The structures of all the complexes were solved by molecular replacement with MOLREP from the CCP4 suite of programs[17] using the Eg5 structure as a search model (PDB code: 1X88). The two molecules in the asymmetric unit were positioned and refined with REFMAC5 using rigid body refinement followed by restrained refinement.[18] The calculation of R_{free} used 5% of

Table 1. Data Collection and Refinement Statistics for Eg5−Inhibitor Complexes

	enastron[a]	dimethylenastron[a]	fluorastrol[a]
unit cell dimensions: a, b, c, β (Å, deg)	69.6, 79.8, 159.3, 90	69.5, 79.7, 159.3, 90	69.6, 79.8, 160.0, 90
space group	$P2_12_12_1$	$P2_12_12_1$	$P2_12_12_1$
beamline	ID23−1	ID23−1	ID14−1
detector	Q315R	Q315R	Q210
molecules per asu	2	2	2
resolution range (Å)	30−1.9	30−2.30	30−2.40
no. of reflections	347 186	314 811	257 554
no. of unique reflections	69 235	40 030	35 497
completeness (%)	98.2 (94.6)	99.9 (99.4)	95.5 (93.4)
multiplicity	5.0	7.9	7.3
R_{sym} (%)	11.8 (34.4)	10.3 (38.6)	9.6 (33.2)
c$I/\sigma(I)$	10.0 (4.9)	16.0 (5.5)	10.8 (5.0)
Wilson B (Å^2)	14.57	28.48	33.70
refinement statistics			
R_{work}/R_{free} (%)	16.31/23.16	17.59/24.05	19.58/27.32
average *B* factors			
overall	19.49	21.42	23.41
main chain/side chain	16.58/21.72	19.58/22.93	21.97/24.67
no. of Mg^{2+}ADP/inhibitor/water	2/2/822	2/2/541	2/2/433
rmsd in bond length (Å)[b]	0.0126	0.0135	0.0133
rmsd in bond angle (deg)	1.502	1.649	1.819

[a] The racemic mixture was used for crystallization of the protein−inhibitor complex. [b] rmsd is the root-mean-square deviation from ideal geometry.

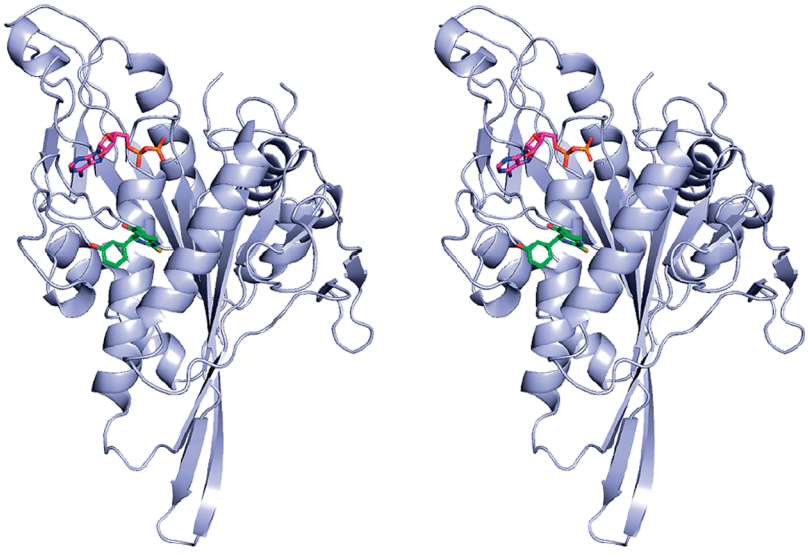

Figure 2. Stereoplot of the overall structure of the Eg5 motor domain with *S*-dimethylenastron bound in the inhibitor-binding pocket. Mg^{2+}ADP and dimethylenastron are shown as stick-and-ball models in red and green respectively.

data. Electron density and difference density maps were all σs_A-weighted, inspected, and the models were rebuilt and improved using Coot.[19] The ligand coordinates and the cif dictionaries for the refinement were obtained using the Dundee PRODRG server.[20] Model geometry was analyzed using PROCHECK[17], and the figures were prepared using PyMOL.[21] Crystallographic statistics for the three crystal structures are given in Table 1.

Tissue Culture. HCT116 (ATCC CCL-247) cells were cultured in DMEM (Invitrogen, Paisley, UK), supplemented with 10% fetal bovine serum (PAA, Pasching, Austria). K562 (ATCC CCL-243) and NCI-H1299 (CRL-5803) cells were cultured in RPMI (Invitrogen, Paisley, UK), supplemented with 10% fetal bovine serum (PAA, Pasching, Austria). BxPC-3 (ATCC CRL-1687) cells were cultured in RPMI (Invitrogen, Paisley, UK), supplemented with 1% nonessential amino acids (Invitrogen, Paisley, UK), 1% sodium pyruvate (Invitrogen, Paisley, UK), 1% glutamine (Invitrogen, Paisley, UK), and 10% fetal bovine serum (PAA, Pasching, Austria). KB-3-1 (DSMZ ACC 158) cells were cultured in DMEM (Invitrogen, Paisley, UK), supplemented with 1% sodium pyruvate (Invitrogen, Paisley, UK), 1% glutamine (Invitrogen, Paisley, UK), and 10% fetal bovine serum (PAA, Pasching, Austria). KB-V1 (DSMZ ACC 149) were cultured in DMEM (Invitrogen, Paisley, UK), supplemented with 1% glutamine (Invitrogen, Paisley, UK) and 15% fetal bovine serum (PAA, Pasching, Austria). To maintain mdr1 mRNA overexpression, media also contained 600 ng/mL of vinblastine. hTERT-HME1 cells (Clontech, Basingstoke, UK) were cultured in Mammary Epithelial Cell Growth Medium (PromoCell, Heidelberg, Germany). All cells were maintained at 37 °C, 95% humidity, and 5% carbon dioxide in a humidified incubator. They were used for experiments for 6−8 weeks before they were replaced with fresh stocks, which are stored in liquid nitrogen.

Cell Proliferation Assays. Cells were seeded in triplicate in 96-well assay plates at 1.250 cells (BxPC-3, HCT116), 2.500 cells (hTERT-HME1, NCI-H1299), or 5.000 cells (K562) per well in 100 μL of the respective growth medium. Medium blanks and cell blanks for every cell line were also prepared. On the next day, inhibitors were added with a starting concentration of 100 μM in a 3-fold serial dilution series. At 72 h post inhibitor addition, 10% Alamar Blue (Invitrogen, Paisley, UK) was added and depending on the cell line, 2−12 h later the absorbance was measured at 570 and 600 nm. All values were corrected for the absorbance of the medium blank and the corrected cell blanks were set to 100%. Calculations for determining the relative proliferation were performed using equations described in the manufacturer's manual. Finally, the EC_{50} values were determined using a sigmoidal dose−response fitting (variable slope) with GraphPad Prism 5.01 for Windows (GraphPad Software, San Diego, USA).

MDR Assays. Cells were seeded in triplicates in 96-well assay plates at 2.000 cells (KB-3-1 and KB-V1) per well in 100 μL of the respective growth medium. For KB-V1, no vinblastine was added for the duration of the assay. To suppress Pgp-overexpression, 1 μM Zosuquidar trihydrochloride (Diverchim, Montataire, France) was added to an additional set of plates. The setup and measurements of the assay are identical to the proliferation assay described before. The MDR ratio was calculated by dividing the EC_{50} value for a particular drug in the mdr1-overexpressing KB-V1 cells by the EC_{50} value obtained in the parental KB-3-1 cells. Thus, if an inhibitor is a substrate for mdr1, KB-V1 cells will be more resistant to its antiproliferative effects than KB-3-1 cells, resulting in an MDR ratio greater than 1. In the presence of the specific Pgp inhibitor Zosuquidar, resistance due to the overexpression of Pgp is abrogated, thus confirming that the efflux by Pgp is indeed responsible for the observed drug resistance. Statistical significance of differences in the EC_{50} values were assessed using ANOVA with GraphPad Prism 5.03 for Windows (GraphPad Software, San Diego, CA).

Results

Overall Structures. We solved the crystal structures of human Eg5 in complex with enastron (Figure 2), dimethylenastron, and fluorastrol. Each Eg5−inhibitor structure was solved in space group $P2_12_12_1$. Statistics for data collection, structure determination, and refinement are summarized in Table 1. All structures contain two molecules per asymmetric unit. Furthermore, the first 15 residues at the N-terminus are missing in all structures. Loop L11 is also absent as in most other kinesin structures. All structures have one molecule of Mg^{2+}ADP bound in the nucleotide-binding pocket with the magnesium coordinated octahedrically with the β-phosphate, the oxygen (OG1) of the hydroxyl side chain of Thr112, and four water molecules. All three inhibitors bind to Eg5 at the well-characterized inhibitor-binding pocket, bordered by helix α2, loop L5, and helix α3. On the basis of the chemical structure, the three distinct inhibitors share a common 3-hydroxyphenyl group, which occupies the same position in all the crystal structures we solved and makes

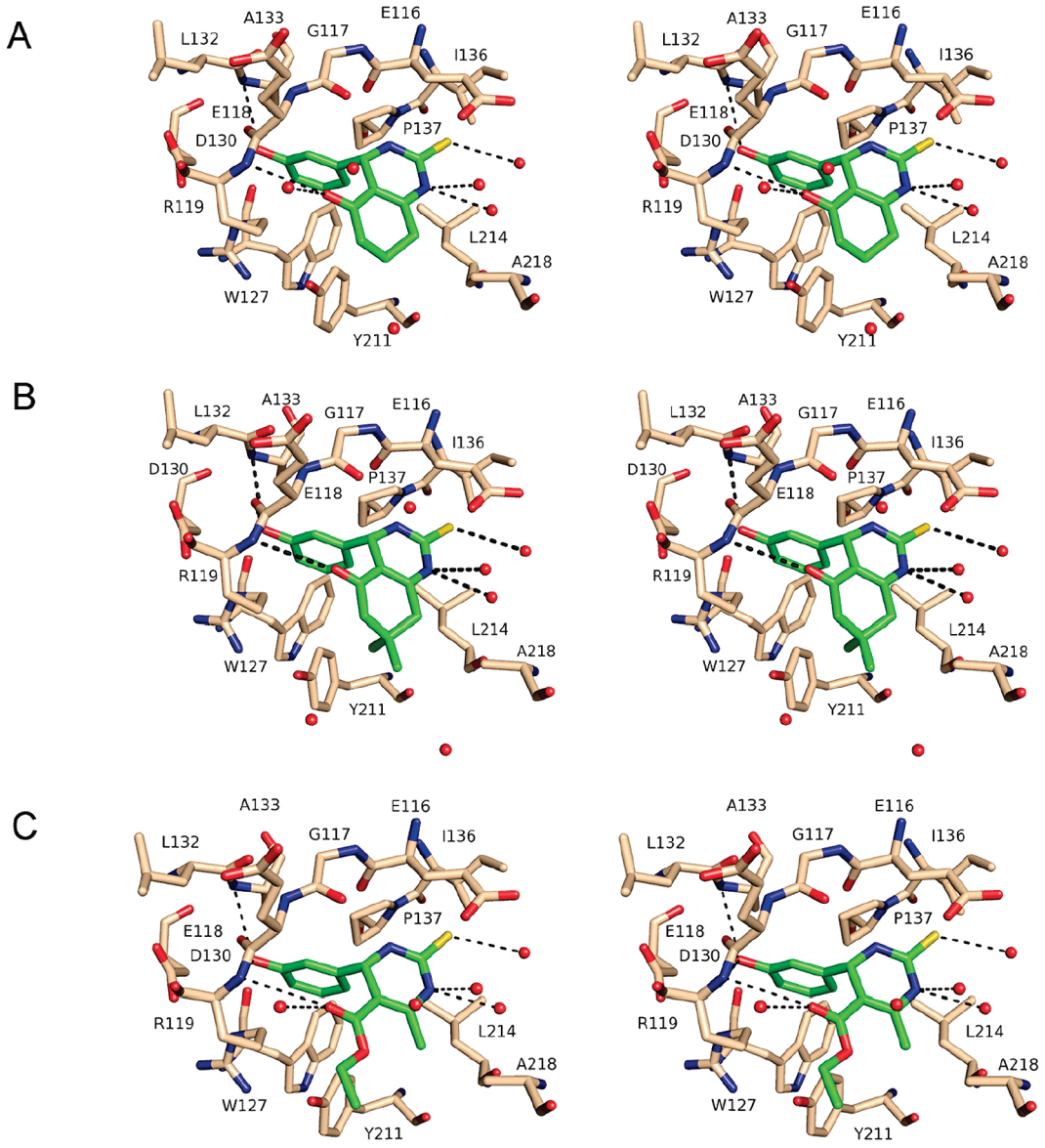

Figure 3. Stereoplots of residues involved in protein−inhibitor interactions. Hydrogen bonds are represented by black broken lines. (A) Eg5−*S*-enastron. (B) Eg5−*S*-dimethylenastron. (C) Eg5−*S*-monastrol.

virtually identical interactions with the residues in the inhibitor-binding pocket.

Eg5−*S*-Enastron Complex. Eg5 was crystallized in the presence of racemic enastron; yet, the obtained structure revealed full occupancy of the inhibitor in the *S*-configuration and there is no evidence for binding in the *R*-configuration (Figure 3A). The 3-hydroxy group on the phenyl ring makes hydrogen bonds with the main chain carbonyl group of Glu118, the main chain amino group of Ala133, and the side chain nitrogen (NE) of Arg119. Moreover, the phenyl ring forms C—H---π interaction with the pyrrolidine ring of Pro137 and edge-to-face (T-shape) interactions with the phenyl rings of Trp127 and Tyr211. Next to the phenol group is the dihydropyrimidine ring. Here, the 2-thioxo group points toward the core of the protein and interacts with one water molecule. In addition, the nitrogen at position 1 (NAK) acts as a hydrogen donor and forms hydrogen bonds with two water molecules. Adjacent to the dihyropyrimidine ring is the oxo-cyclohexene ring system. The oxygen acts as a hydrogen bond acceptor and forms a hydrogen bond with the main chain amino group of Arg119 and with a structural water molecule.

Eg5−*S*-Dimethylenastron Complex. We used the racemic mixture of dimethylenastron for crystallization with Eg5. The structure indicates a preference of Eg5 for the *S*-enantiomer instead of the *R*-enantiomer. The overall conformation of dimethylenastron in the inhibitor-binding pocket (Figure 3B) and the interactions with the residues of the allosteric binding site is virtually identical to that observed with enastron. The only difference between the Eg5−enastron and Eg5−dimethylenastron complex is the additional dimethyl groups on the oxo-cyclohexene ring system, which points toward the solvent region but maintains hydrophobic interactions ($\leq$3.9 Å) with the hydrophobic main chain of Ala218 that constitutes part of helix α3. In addition, one of the methyl groups (CAA) makes significant C—H---π interactions with Tyr211.

Eg5−*R*-Fluorastrol Complex. We crystallized Eg5 with the racemic mixture of fluorastrol and observed that it binds preferentially to Eg5 in the *R* configuration, unlike monastrol (Figure 3C), enastron, and dimethylenastron, which bind in

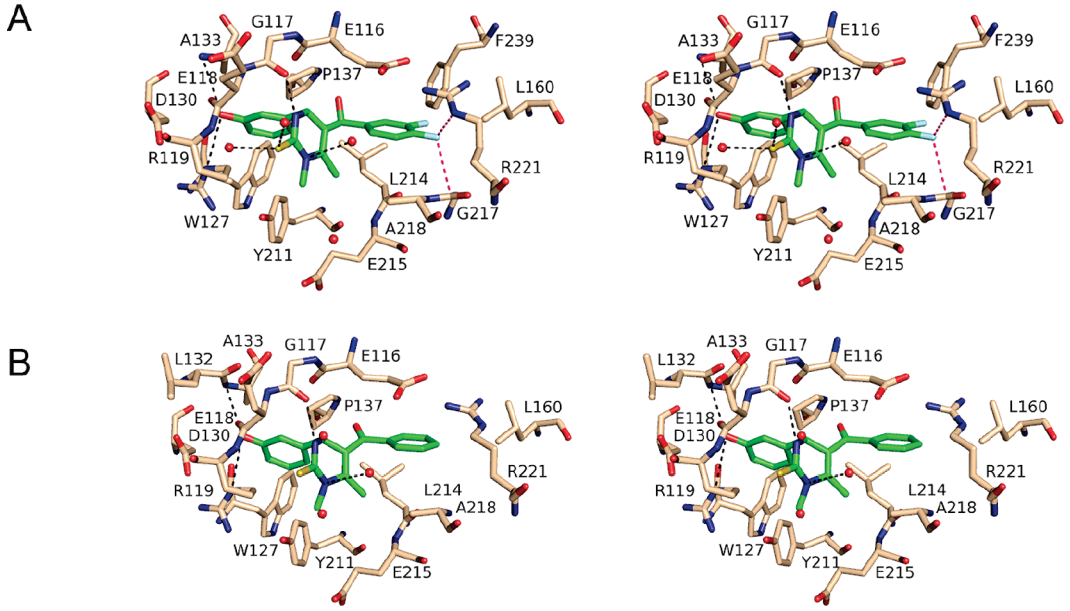

Figure 4. Stereoplots of residues involved in protein−inhibitor interactions. Hydrogen bonds are represented by black broken lines, while multipolar interactions are shown in pink broken lines. (A) Eg5−*R*-fluorastrol. (B) Eg5−*R*-mon-97.

Table 2. Growth Inhibition Assays of Monastrol-Like Compounds Conducted in Different Tumor and Nontumor Cell Lines

	EC_{50} [nM]				
compd	HCT116	hTERT-HME1	BxPC3	K562	NCI-H1299
rac-monastrol	24155 ± 2848	45082 ± 21354	> 100 μM	> 100 μM	> 100 μM
rac-enastron	1811 ± 175	2443 ± 245	2072 ± 483	4775 ± 337	4898 ± 392
rac-dimethylenastron	330 ± 17	603 ± 44	743 ± 104	769 ± 71	881 ± 64
rac-**1**	951 ± 113	2541 ± 247	2158 ± 403	2624 ± 398	2393 ± 202
rac-**2**	1294 ± 55	2818 ± 423	2838 ± 725	2735 ± 290	2773 ± 254
rac-fluorastrol	387 ± 22	247 ± 42	601 ± 105	1149 ± 46	1355 ± 81
fluorastrol-E1	15171 ± 1582	> 100 μM	33651 ± 10182	26607 ± 1465	32961 ± 2197
fluorastrol-E2	327 ± 54	223 ± 48	736 ± 91	820 ± 20	783 ± 25
rac-mon97	1832 ± 182	1778 ± 140	5000 ± 671	5688 ± 648	6887 ± 487
mon97-E1	6502 ± 487	> 50000	14421 ± 1753	11405 ± 671	18076 ± 1016
mon97-E2	1740 ± 111	1187 ± 87	3597 ± 193	3695 ± 507	4608 ± 177

the *S* configuration. Consequently, the interactions in the inhibitor-binding pocket, apart from that of the 3-hydroxyphenyl group which is common in all three inhibitors, are strikingly different from that of enastron and dimethylenastron. In the *R* configuration, the 2-thioxo group points to the solvent-exposed region of the protein and interacts with two water molecules (Figure 4A). The N1−H on the dihydropyrimidine ring interacts with a water molecule, and the N3−H group interacts via a hydrogen bond with the main chain carbonyl group of Gly117. The 3′,4′-difluorophenyl group, on the other hand, points toward the core of the protein. One of the fluorines (FAF) forms multipolar interactions[22] with the guanidinium side chain of Arg221, the main chain amide of Ala218 and the main chain carbonyl group of G217. In this configuration, the other fluorine (FAG), which points toward the edge of the phenyl ring of Phe239, and the carbonyl group (OAC) of the inhibitor do not form any hydrogen bond interactions with the rest of the protein.

Activity of Monastrol-Like Compounds in Different Cell Lines. To be able to directly compare DHPM analogues developed by different groups, we investigated 11 compounds in proliferation assays in five different cell lines, including four tumor cell lines and one nontransformed (normal) cell line (Table 2). Monastrol was included as a control and was a weak inhibitor throughout all cell lines. Expectedly, dimethylenastron is a stronger inhibitor than enastron and is approximately 6-fold more potent. Although there are some intercellular variations between racemic dimethylenastron and racemic fluorastrol, both compounds are almost equally potent, with the best EC_{50} values reaching about 300 nM in the colon cancer cell line HCT116. These compounds are also very active in the untransformed breast cancer cell line hTERT-HME1. Fluorastrol is about 5-fold more active than mon-97 when comparing the racemic mixtures and the more active enantiomers. Comparison of the racemic mixture of fluorastrol with **1** and **2** (Figure 1) reveals that analogues with only one fluorine in either the *meta*-(**2**) or *para*-position (**1**) are less active in cell-based assays than analogues with two fluorines (fluorastrol). Comparison of the enantiomers of fluorastrol also clearly indicates that the *R*-enantiomer is at best about 30-fold more potent than the *S*-enantiomer.

MDR Ratio. To identify whether or not the investigated DHPMs are substrates for P-glycoprotein (Pgp), we determined the MDR ratios for the two most potent racemic analogues, *rac*-dimethylenastron and *rac*-fluorastrol. Vinblastine, a known Pgp substrate and monastrol, which had previously been shown to be a bad substrate for Pgp,[23] were

Table 3. Determination of MDR Ratios for the Two Most Potent Class I and Class II DHPMs, *rac*-Dimethyleastron and *rac*-Fluorastrol, Respectively, Using a Proliferation Assay with Human Cervix Carcinoma KB-V1 Cells, Overexpressing mdr1 at Both the mRNA and Protein Level and Its Parental Cell Line KB-3-1[a]

	EC_{50} [nM]				
compd/cell line	KB-3-1	KB-3-1+Z	KB-V1	KB-V1+Z	MDR ratio
vinblastine	12.6 ± 2.0	8.5 ± 0.7	2 037 ± 135	13.0 ± 0.7	162
rac-monastrol	85114 ± 12170	56494 ± 7132	99083 ± 14716	45394 ± 10760	1.2
rac-dimethylenastron	661 ± 45	594 ± 94	12 303 ± 2 824	434 ± 35	18.6
rac-fluorastrol	832 ± 88	800 ± 246	2 084 ± 285	671 ± 123	2.5

[a] Vinblastine and monastrol were used as positive and negative controls, respectively. Zosuquidar (Z) was used as a specific inhibitor of Pgp; thus, abrogating its effect on drug efflux.

used as controls (Table 3). *rac*-Fluorastrol shows an MDR ratio of 2.5, indicating that this compound is, if at all, a moderate substrate for Pgp. In contrast, *rac*-dimethylenastron, which overall is a slightly more potent inhibitor of Eg5 in cell-based assays, shows an MDR ratio of 18.6, a more than 7-fold difference; thus, *rac*-dimethylenastron would be a good substrate for Pgp (Supporting Information).

Discussion

Comparison of Monastrol, Enastron, and Dimethylenastron. On the basis of the in vitro assays done by Gartner et al.,[11] enastron (IC_{50} = 2 μM) and dimethylenastron (IC_{50} = 200 nM) have been shown to be 10- and 100-times more potent than monastrol (IC_{50} = 30 μM). By comparing the crystal structures of Eg5 in complex with each of the three inhibitors, we hope to understand how the structural differences of the three inhibitors could contribute to the varying levels of potency. Upon overlaying the Eg5−enastron and Eg5−dimethylenastron structures with Eg5−monastrol,[9] we observed no difference in the positions of the three inhibitors in the allosteric binding site. The interactions between the inhibitors and the residues in the inhibitor-binding pocket are also virtually identical. The only striking difference is that enastron and dimethylenastron have the oxo-cyclohexene system, while monastrol has a C5-ester group. In Figure 3C, we show that the ester group of monastrol extends out of the allosteric binding site into the solvent-exposed region but does not completely fill the space in the solvent-exposed subpocket. On the basis of our crystal structures, we concur with Gartner et al. that the cyclization of the side chain, resulting in a cyclic ketone, confers rigidity to the conformation of the inhibitor. This results in the better fit of the inhibitor in the solvent-exposed subpocket formed by Glu215, Tyr211, and Arg119, as observed in the Eg5−enastron complex. In view of the small structural difference, namely the two methyl groups, between enastron and dimethylenastron, it seems surprising that the latter is about six times more active than enastron in vitro and in cell-based assays. The increase in potency would most likely be due to the C—H---π interaction that one of the methyl groups forms with Tyr211. In addition, the dimethyl group of dimethylenastron occupies the space of the solvent-exposed subpocket with a better fit to the allosteric binding site than enastron. This better fit was also reflected by the higher docking scores for dimethylenastron.[13]

Comparison between Mon-97 and Fluorastrol. By comparing the crystal structure of Eg5−fluorastrol to that of a structurally similar inhibitor mon-97,[10] we can try to understand the reason behind the significant 5-fold increase in potency in cell-based assays. Upon overlaying the two structures, we observed no difference in position of the main scaffold or interactions of the two inhibitors with the rest of the protein. The only difference between the two inhibitors is the two fluorines that are attached to the phenyl ring in the *meta*- and *para*-positions. One of these fluorines plays a very important role in forming multipolar interactions with the residues at the allosteric binding site (Figure 4A), while the other fluorine points toward Phe239. Additionally, the aromatic ring stacks with the salt-bridge formed by the side chain resides of Glu116 and Arg221. The two fluoro atoms and the carbonyl group withdraw electron density from the phenyl ring by inductive and mesomeric effects, respectively. Thus, the fluorine atoms, bearing higher electron density, are closer to the positively charged side chain of Arg221 and the electron-poor edge of Phe239, while the phenyl ring that has lower electron density is closer to the negatively charged side chain of Glu116. This explains the overall improved affinity of this compound.

There have been previous examples, where the addition of fluorines to lead compounds has beneficial effects on the physicochemical properties of the drug and strengthened the protein−ligand interactions, as evident from other major fluorinated drugs: Prozac, an antidepressant, and Lipitor, a cholesterol-lowering drug.[22] While analogues with only one fluorine in either the *meta*-(**2**) or *para*-position (**1**) are more active than mon-97 in cell-based assays, the incorporation of both fluorines lead to the highly improved activity of fluorastrol (Table 2).

Stereoselectivity of Enastron and Dimethylenastron. For the improvement of small molecule inhibitors, it is essential to understand the stereoselectivity of the compound. Yet, little is known about the stereoselectivity of DHPM inhibitors such as enastron and dimethylenastron; thus, we crystallized the racemic mixture of these two inhibitors with Eg5. As enastron and dimethylenastron are analogues of monastrol, they are also structurally very similar to it. For all three inhibitors, the *S*-enantiomer was found to bind preferentially to Eg5 in the respective crystal structures. Therefore, we predict that the *S*-enantiomer of enastron and dimethylenastron, rather than the *R*-enantiomer, is the active agent. Thus, they belong to class I of DHPM inhibitors that bind in the *S* configuration, similar to monastrol.

Stereoselectivity of Fluorastrol. Though all three small molecules, enastron, dimethylenastron, and fluorastrol, are DHPM inhibitors, they exhibit different stereoselectivity. While enastron and dimethylenastron bind preferentially to Eg5 in the *S* configuration, fluorastrol binds preferentially in the *R* configuration. When using the racemic mixture of fluorastrol for crystallization, the conformation of the inhibitor and its interaction with the protein, as revealed by the crystal structure, is virtually identical to that obtained from the *R*-enantiomer. This confirms the strong preference of Eg5 for the *R*-enantiomer over the *S*-enantiomer. In fact, we have

previously solved the structure of the Eg5-mon-97 complex at 2.7 Å resolution and found that mon-97 belongs to a different class of DHPM inhibitors, as it binds preferentially in the *R* configuration[10] (Figure 4B). Now that we have solved the structure of Eg5 in complex with fluorastrol to a higher resolution (2.4 Å), we can confirm this unexpected change in configuration and conclude that fluorastrol is a class II DHPM inhibitor, just like mon-97. Therefore, the crystal structure of the Eg5−fluorastrol complex supports the fact that the *R*-enantiomer is the more active agent. This finding is also backed by the results of in vitro[13] and cell-based assays.

MDR Study. The hallmark of Pgp is its capacity to accept a wide range of structurally diverse chemical compounds as substrates. Thus, defining a Pgp substrate can be quite complex. Given that some of the characteristics of a typical Pgp substrate, including the presence of nitrogen groups and aromatic rings, are found in our inhibitors, we decided to carry out an MDR study to find out whether they may be substrates of Pgp. However, our results clearly demonstrate that one of the two most potent analogues in our study, *rac*-fluorastrol, has an MDR ratio below 10, which according to Cox et al. would probably have the potential to overcome MDR and hence worth pursuing.[24,25] On the other hand, *rac*-dimethylenastron, which has an MDR ratio above 10, would probably be a good substrate for Pgp.

Coordinate Files. Coordinates and structure factors for Eg5-*S*-enastron (PDB ID: 2X7C), Eg5-*S*-dimethylenastron (PDB ID: 2X7D), and Eg5-*R*-fluorastrol complexes (PDB ID: 2X7E) were deposited at the Protein Data Bank.

Conclusion

To better understand how small molecule inhibitors interact with Eg5 at the structural level and to confirm the unusual binding configuration of compound mon-97, we determined the structures of three DHPM analogues: enastron, dimethylenastron, and fluorastrol. We observed that the 3-hydroxyphenyl group, the only common functional moiety, remains conformationally unchanged between the three inhibitors and has virtually identical interactions with the residues of Eg5. By comparing these crystal structures to that of monastrol and mon-97, we identified the main reasons for increased potency of these new inhibitors, namely the better fit of the ligand to the allosteric binding site for enastron and dimethylenastron and the addition of two fluorine atoms for fluorastrol. We also showed that monastrol, enastron, and dimethylenastron belong to class I DHPM inhibitors that bind in the *S* configuration, whereas mon-97 and fluorastrol are class II DHPM inhibitors that bind preferentially in the *R* configuration. With these new structural evidence for the stereoselectivity of DHPM inhibitors, the possibilities for future structure-based drug design is considerably expanded.

For future work, we suggest separating the racemic mixtures of potential compounds into their separate enantiomers to identify the more active biological agent. As for the improvement of these compounds, we propose keeping the 3-hydroxyphenyl group as it forms important hydrogen bond interactions with the residues in the pocket. The 3′,4′-difluorophenyl group, which points toward the core of the protein, is also a main contributing factor to the potency of the class II inhibitors. As we discovered from the Eg5−enastron and Eg5−dimethylenastron structures, a bulky, cyclic functional group, which fully occupies the solvent-exposed subpocket near Tyr211, results in a better fit and an increase in potency of the class I inhibitors. The next logical step would be to merge these two optimized interaction patterns of class I and II DHMP inhibitors, preferably by modification of the class II scaffold. Taking into account all the observations from the various crystal structures described in this paper, we now have a basis for structure-guided optimization of DHPM inhibitors that will lead to compounds with improved drug-like properties and potency.

Acknowledgment. We thank Dr. Sandor Bruckhauser for his support at the ESRF beamlines ID14-1, ID-23, and ID29. We are grateful to Dr. Christian Laggner (University of Innsbruck) for his insightful comments on the manuscript and Dr. Zbigniew Dauter (Argonne National Laboratory, National Cancer Institute, USA) for helpful discussions. Kristal Kaan holds a National Science Scholarship, financed by A*STAR (Singapore), and this publication contains part of her doctoral thesis. We thank Cancer Research UK for financial support.

Supporting Information Available: EC_{50} graphs used in the determination of MDR ratios. This material is available free of charge via the Internet at http://pubs.acs.org.

References

(1) Blangy, A.; Lane, H. A.; d'Herin, P.; Harper, M.; Kress, M.; Nigg, E. A. Phosphorylation by p34cdc2 regulates spindle association of human Eg5, a kinesin-related motor essential for bipolar spindle formation in vivo. *Cell* **1995**, *83*, 1159–1169.
(2) Cole, D. G.; Saxton, W. M.; Sheehan, K. B.; Scholey, J. M. A "Slow" homotetrameric kinesin-related motor protein purified from *Drosophila* embryos. *J. Biol. Chem.* **1994**, *269*, 22913–22916.
(3) Sawin, K. E.; LeGuellec, K.; Philippe, M.; Mitchison, T. J. Mitotic spindle organization by a plus-end-directed microtubule motor. *Nature* **1992**, *359*, 540–543.
(4) Weil, D.; Garcon, L.; Harper, M.; Dumenil, D.; Dautry, F.; Kress, M. Targeting the kinesin Eg5 to monitor siRNA transfection in mammalian cells. *Biotechniques* **2002**, *33*, 1244–1248.
(5) Mayer, T. U.; Kapoor, T. M.; Haggarty, S. J.; King, R. W.; Schreiber, S. L.; Mitchison, T. J. Small molecule inhibitor of mitotic spindle bipolarity identified in a phenotype-based screen. *Science* **1999**, *286*, 971–974.
(6) Wilson, L.; Jordan, M. A. New microtubule/tubulin-targeted anticancer drugs and novel chemotherapeutic strategies. *J Chemother.* **2004**, *16* (Suppl 4), 83–85.
(7) Rowinsky, E. K.; Chaudhry, V.; Cornblath, D. R.; Donehower, R. C. Neurotoxicity of Taxol. *J. Natl. Cancer Inst. Monogr.* **1993**, 107–115.
(8) Huszar, D.; Theoclitou, M. E.; Skolnik, J.; Herbst, R. Kinesin motor proteins as targets for cancer therapy. *Cancer Metastasis Rev.* **2009**, *28*, 197–208.
(9) Yan, Y.; Sardana, V.; Xu, B.; Homnick, C.; Halczenko, W.; Buser, C. A.; Schaber, M.; Hartman, G. D.; Huber, H. E.; Kuo, L. C. Inhibition of a mitotic motor protein: where, how, and conformational consequences. *J. Mol. Biol.* **2004**, *335*, 547–554.
(10) Garcia-Saez, I.; DeBonis, S.; Lopez, R.; Trucco, F.; Rousseau, B.; Thuery, P.; Kozielski, F. Structure of human Eg5 in complex with a new monastrol-based inhibitor bound in the R configuration. *J. Biol. Chem.* **2007**, *282*, 9740–9747.
(11) Gartner, M.; Sunder-Plassmann, N.; Seiler, J.; Utz, M.; Vernos, I.; Surrey, T.; Giannis, A. Development and biological evaluation of potent and specific inhibitors of mitotic Kinesin Eg5. *ChemBioChem* **2005**, *6*, 1173–1177.
(12) Sarli, V.; Huemmer, S.; Sunder-Plassmann, N.; Mayer, T. U.; Giannis, A. Synthesis and biological evaluation of novel EG5 inhibitors. *ChemBioChem* **2005**, *6*, 2005–2013.
(13) Prokopcová, H., Dallinger, D., Uray, G., Kaan, H. Y. K., Ulaganathan, V., Kozielski, F., Laggner, C., Kappe, C. O. Structure−Activity Relationships and Molecular Docking of Novel Dihydropyrimidine-Based Mitotic Eg5 Inhibitor. Unpublished results.
(14) Kaan, H. Y.; Ulaganathan, V.; Hackney, D. D.; Kozielski, F. An allosteric transition trapped in an intermediate state of a new kinesin-inhibitor complex. *Biochem. J.* **2010**, *425*, 55–60.

(15) Otwinowski, Z.; Minor, W. [20] Processing of X-ray diffraction data collected in oscillation mode. In *Methods in Enzymology*; Academic Press: New York, 1997; Vol. 276, p 307.
(16) Powell, H. R. The Rossmann Fourier autoindexing algorithm in MOSFLM. *Acta Crystallogr., Sect. D: Biol. Crystallogr.* **1999**, *55* (Pt 10), 1690–1695.
(17) Collaborative Computational Project, N. The CCP4 Suite: Programs for Protein Crystallography. *Acta Crystallogr.* **1994**, 760−763
(18) Murshudov, G. N.; Vagin, A. A.; Dodson, E. J. Refinement of macromolecular structures by the maximum-likelihood method. *Acta Crystallogr., Sect. D: Biol. Crystallogr.* **1997**, *53*, 240–255.
(19) Emsley, P.; Cowtan, K. Coot: model-building tools for molecular graphics. *Acta Crystallogr., Sect. D: Biol. Crystallogr.* **2004**, *60*, 2126–2132.
(20) Schuttelkopf, A. W.; van Aalten, D. M. PRODRG: a tool for high-throughput crystallography of protein−ligand complexes. *Acta Crystallogr., Sect. D: Biol. Crystallogr.* **2004**, *60*, 1355–1363.
(21) DeLano, W. L. *The PyMOL Molecular Graphics System*; DeLano Scientific: San Carlos, CA, 2002.
(22) Muller, K.; Faeh, C.; Diederich, F. Fluorine in pharmaceuticals: looking beyond intuition. *Science* **2007**, *317*, 1881–1886.
(23) Peters, T.; Lindenmaier, H.; Haefeli, W. E.; Weiss, J. Interaction of the mitotic kinesin Eg5 inhibitor monastrol with P-glycoprotein. *Naunyn-Schmiedeberg's Arch. Pharmacol.* **2006**, *372*, 291–299.
(24) Cox, C. D.; Breslin, M. J.; Whitman, D. B.; Coleman, P. J.; Garbaccio, R. M.; Fraley, M. E.; Zrada, M. M.; Buser, C. A.; Walsh, E. S.; Hamilton, K.; Lobell, R. B.; Tao, W.; Abrams, M. T.; South, V. J.; Huber, H. E.; Kohl, N. E.; Hartman, G. D. Kinesin spindle protein (KSP) inhibitors. Part V: discovery of 2-propylamino-2,4-diaryl-2,5-dihydropyrroles as potent, water-soluble KSP inhibitors, and modulation of their basicity by beta-fluorination to overcome cellular efflux by P-glycoprotein. *Bioorg. Med. Chem. Lett.* **2007**, *17*, 2697–2702.
(25) Cox, C. D.; Coleman, P. J.; Breslin, M. J.; Whitman, D. B.; Garbaccio, R. M.; Fraley, M. E.; Buser, C. A.; Walsh, E. S.; Hamilton, K.; Schaber, M. D.; Lobell, R. B.; Tao, W.; Davide, J. P.; Diehl, R. E.; Abrams, M. T.; South, V. J.; Huber, H. E.; Torrent, M.; Prueksaritanont, T.; Li, C.; Slaughter, D. E.; Mahan, E.; Fernandez-Metzler, C.; Yan, Y.; Kuo, L. C.; Kohl, N. E.; Hartman, G. D. Kinesin spindle protein (KSP) inhibitors. 9. Discovery of (2*S*)-4-(2,5-difluorophenyl)-*n*-[(3*R*,4*S*)-3-fluoro-1-methylpiperidin-4-yl]-2-(hydroxymethyl)-*N*-methyl-2-phenyl-2,5-dihydro-1*H*-pyrrole-1-carboxamide (MK-0731) for the treatment of taxane-refractory cancer. *J. Med. Chem.* **2008**, *51*, 4239–4252.